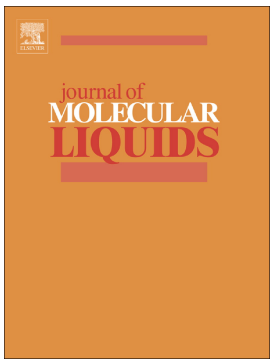


# Role of a cystine-based Gemini surfactant ligand in the synthesis of catalytic active silver nanoparticles

María Andrea Molina Torres, Erica Marcela Pachón Gómez, Mariana Adela Fernández, Alicia Viviana Veglia, Natalia Lorena Pacioni

PII: S0167-7322(19)31197-3
DOI: https://doi.org/10.1016/j.molliq.2019.03.168
Reference: MOLLIQ 10709

To appear in: *Journal of Molecular Liquids*

Received date: 28 February 2019
Revised date: 27 March 2019
Accepted date: 29 March 2019

Please cite this article as: M.A.M. Torres, E.M.P. Gómez, M.A. Fernández, et al., Role of a cystine-based Gemini surfactant ligand in the synthesis of catalytic active silver nanoparticles, Journal of Molecular Liquids, https://doi.org/10.1016/j.molliq.2019.03.168

# Role of a Cystine-based Gemini Surfactant Ligand in the Synthesis of Catalytic Active Silver Nanoparticles

María Andrea Molina Torres[a,b], Erica Marcela Pachón Gómez[a,b], Mariana Adela Fernández[a,b], Alicia Viviana Veglia[a,b] and Natalia Lorena Pacioni[a,b]*

[a]*Universidad Nacional de Córdoba, Facultad de Ciencias Químicas, Departamento de Química Orgánica. Haya de la Torre y Medina Allende s/n, X5000HUA, Ciudad Universitaria, Córdoba, Argentina.*

[b]*Consejo Nacional de Investigaciones Científicas y Técnicas (CONICET), INFIQC, Cordoba, Argentina.*

*Phone: +54-351-5353867 ext 55374*

*Emails: amolinatorres@fcq.unc.edu.ar; ericapachog@gmail.com; marfer@fcq.unc.edu.ar, aveglia@fcq.unc.edu.ar*

Corresponding author*: nataliap@fcq.unc.edu.ar*

**Abstract**[&]

We report the synthesis in water of colloidal silver nanoparticles (AgNP) using a Gemini lipoamino acid surfactant derived from cysteine as a capping agent. The Gemini surfactant interacts with the metal surface mainly in a monodentate vertical mode through the carboxylate group preserving intact the disulfide bond. These nanoparticles present catalytic activity to the reduction of *p*-nitrophenol, and the synthesis of AgNP under mild reduction conditions maintaining the seeds size. Also, the Gemini surfactant leads to anisotropic morphologies in the seed-mediated growth of AgNP@citrate seeds aided by the presence of bromide ions.

**Keywords**

**silver nanoparticles; Gemini lipoamino acid surfactant; seed-mediated growth; catalysis; p-nitrophenol reduction**



[&] **Abbreviations**: **AgNP** silver nanoparticles; **cmc** critical micelle concentration; **DLS** Dynamic Light Scattering; **DTG** Derivative Thermogravimetric curves; **FWHM** full width at half maximum; **GS** gemini surfactant; **sd** standard deviation; **SDDC** sodium didecamido cystine; **SPR** Surface Plasmon Resonance; **TEM** Transmission Electron Microscopy; **TGA** Thermogravimetric Analysis.

## 1. Introduction

Nowadays, silver nanoparticles (AgNP) play a remarkably role due to their several applications in optical devices, catalysis, biomedicine, and sensing [1,2]. Besides, the importance of ligands on the metal surface, acting not only as capping and stabilizing agents, but also defining physical and chemical properties of nanomaterials is well recognized [3–9]. Within this frame, obtaining AgNP using surfactants as ligands can lead to different characteristic features or enhanced properties, for example, they can exert shape control during nanoparticles growth [10], affect their aggregation rates [11], and also tune plasmonic responses [12,13].

Gemini surfactants (**GS**) containing two hydrophobic chains and two hydrophilic heads separated by a spacer bound covalently are known for their improved properties, compared to their monomeric counterparts, like a lower critical micelle concentration (cmc) [14,15]. Commonly, the **GS** chemical structure is indicated using $C_m$-$C_s$-$C_m$ where, *m* and *s* mean the number of carbons in the alkyl side chain and the methylene spacer, respectively. Amino acid-based **GS** present in many cases additional advantages such as, being eco-friendly, biodegradable, non-toxic and water soluble which make them attractive for cosmetics, pharmaceutical, and biomedical applications [16,17]. Thus, the use of natural amino-acid based **GS** as capping agents of AgNP is worthwhile to explore as it might confer different or enhanced properties.

The use of **GS** as ligands in the synthesis of AgNP is still scarce with most examples involving cationic **GS** (Table S1 in the Supplementary material). For instance, in pioneer work, Xu *et al.* [18] obtained monodisperse and stabilized spherical AgNP under reverse micelle conditions using a cationic **GS** referred to as 18-3(OH)-18. Besides, using $C_m$-2-$C_m$ **GS** with different hydrocarbon chain lengths, Bakshi [19] found the shorter one (*m*: 10) favoured the formation of nanorods at low seed concentrations during the seed-mediated growth of AgNP@citrate, while longer alkyl chains (*m*: 12 and 14) induced nanoribbons. In contrast, when the 12-2-12 **GS** was the capping agent during the synthesis, He *et al.* [20] achieved AgNP spheres with good catalytic activity. Further, Battacharya *et al.* [21] using

16-$C_s$-16 **GS** observed the shorter spacers (*s*: 2 and 4) promoted the synthesis of nanorods. Also, a few examples show the ability of anionic **GS** to stabilize AgNP (Table S1), for instance, Negm *et al.* [22] utilized **GS** with phosphate polar heads and a polyethylene glycol spacer to exchange the citrate as ligand and improve the NP stabilization. Recently, Srivastava *et al.*[23] used mixed micelles as capping agents of AgNP and found the higher the proportion of anionic **GS** in the micelle prevented NP aggregation and; Cheng *et al.* [24] obtained microparticles with good Surface Enhanced Raman activity using a $C_m$-Ar-$C_m$ anionic **GS** and a mild reducing agent.

In this work, we depict the synthesis and characterization of AgNP when the ligand is an anionic Gemini lipoamino acid surfactant composed of cystine (dimeric cysteine, Cys) as both polar head and spacer, and decadecyl hydrophobic tails named sodium didecamido cystine, 10-Cys-Cys-10 (Scheme 1, SDDC). We evaluated the catalytic performance of these AgNP@SDDC using as a model reaction to the reduction of 4-nitrophenol. Further, we examined the effect of SDDC in the seed-mediated growth of AgNP@citrate and AgNP@SDDC in order to assess the surfactant ability in shape and size control.

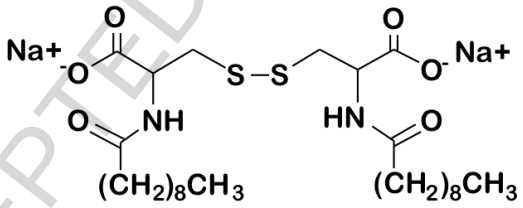


**Scheme 1**. Chemical structure for SDDC

## 2. Materials and methods

### *2.1 Reactants.*

Analytical grade $AgNO_3$ (BioPack), Sodium borohydride (Tetrahedron), *p*-nitrophenol (Aldrich), NaOH (95%, Cicarelli), sodium citrate (Anedra), L-ascorbic acid (Anedra), KBr (Merck) were used as received. 3,3′-disulfanediyl bis 2-decamido propanoic acid (SDDC) was synthesized and characterized

in the laboratory according to the literature [15] by the reaction of cystine with decanoic chloride as described previously [25]. Water was MilliQ quality obtained from a Millipore instrument (resistivity, 25°C: 18 MΩ cm).

### *2.2 Instrumentation.*

All absorption spectra were measured in a UV–vis Shimadzu 1800 spectrophotomer in the 200–800 nm wavelength range using quartz cells (1 cm path-length). Transmission Electron Microscopy images were obtained using a TEM-Jeol 1120 electron microscope, 80 kV accelerating voltage on Carbon-coated copper grids (300 mesh, Electron Microscopy). Zeta potentials were measured in a Delsa$^{TM}$ Nano S Particle Analyzer (Beckman Coulter) at room temperature. Centrifugation was performed in an Eppendorf Centrifuge 5804. Infrared spectra (FT-IR) were recorded in a Nicolet iN10-Microscope: 16 scans, 16 $cm^{-1}$ resolution, sample gain 1.0, aperture 80; Thermogravimetric analysis (TGA) was performed on a thermogravimetric analyser equipment Hi-Res 145 Modulated TGA 2950 under $N_2$ atmosphere in the range 50ºC - 600ºC at a 10ºC/min rate. Raman spectra were measured in a Horiba LabRaman confocal microscope with a 100 × (NA = 0.12) objective in the backscattering geometry. 10 s was the exposition time with a 4 $cm^{-1}$ resolution and 10 or 20 accumulations were obtained for SDDC and for AgNP@SDDC, respectively. The irradiation wavelength used were 514 nm for SDDC and 633 nm for AgNP@SDDC corresponding to the laser lines from Argon and He-Ne, respectively. X-Ray photoelectron spectra were obtained using a K-Alpha X-ray Photoelectron Spectrometer (Thermo Fisher Scientific) with monochromatized Al-Kα X-ray source hν = 1486.6 eV. Survey and high-resolution spectra were collected using 150, 13 (for C) and 50 (for O, S, Ag and N) eV pass energy, respectively. HR-XPS spectra were fitted with XPST software package for Igor Pro 8.02® (WaveMetrics, Inc.) using Gaussian-Lorentzian functions (70%:30%). Due to remaining charging effects through these measurements, we used the C 1s binding energy for aliphatic carbons (284.8 eV) as reference and corrected all spectra accordingly.

### *2.3 Synthesis of AgNP@SDDC*

In an Erlenmeyer flask, we added 0.6 mL aqueous $NaBH_4$ (10.00 mM) in 0.1 mL aliquots every 30 s to a 20 mL aqueous solution containing 0.25 mM $AgNO_3$ and 2.5 mM SDDC under vigorous magnetic stirring at room temperature. Immediately, upon $NaBH_4$ addition, the solution colour became dark brown. The stirring continued for 30 s more after addition of $NaBH_4$. Then, we centrifuged the nanoparticles at 4000 rpm equivalent to a relative centrifugal force (rcf) of 2057×g for 30 min. The pellet was resuspended in 4.0 mL MilliQ water.

### *2.4 Seed-mediated AgNP synthesis in the presence of SDDC*

Besides the AgNP@SDDC seeds, we also synthesized AgNP@citrate seeds as follows: In an Erlenmeyer flask, we added 0.6 mL aqueous $NaBH_4$ (10.00 mM) in 0.1 mL aliquots every 30 s to a 20 mL aqueous solution containing 0.25 mM $AgNO_3$ and 0.25 mM sodium citrate under vigorous magnetic stirring at room temperature. Immediately, upon $NaBH_4$ addition, the solution colour became yellow. The stirring continued for 30 s more after addition of $NaBH_4$. These seeds stood at least 2 hours before use. In the meantime, we prepared growth solutions containing SDDC (3 mM), $AgNO_3$ (0.23 mM) and ascorbic acid (7.2 mM) in that given order. Then, we added 125 μL of seeds aged for 2 h or 24 h (AgNP@citrate or AgNP@SDDC) followed by addition of NaOH (9.1 mM). To chosen solutions, we added KBr. The samples reacted for 48 h before centrifugation and analysis.

### *2.5 Characterization of nanoparticles*

We determined particle size distributions using TEM images of 20 μL colloidal solutions delivered onto 300 mesh carbon-coated copper grids before drying under air. We analysed all the images using ImageJ® software and counting around 200-1000 particles. We measured the absorption

spectra to ascertain the maximum wavelength ($\lambda_{max}$) for the surface Plasmon resonance (SPR) band and its full width at half maximum (FWHM). Also, we calculated the molar absorption coefficient in water and measured the zeta potential (ξ). The zeta potential was determined using the zeta potential cell of the DelsaTM Nano S Particle Analyzer. The cell was rinsed several times with ethanol, water and filled with ~ 0.7 mL of AgNP@SDDC dispersed in MilliQ water at room temperature. The reported zeta potential is the average of five independent measurements.

About the presence of SDDC as the capping agent we recorded the FTIR spectra for SDDC and AgNP@SDDC of solid samples on a KBr disk, and we estimated the amount of SDDC on the nanoparticles performing TGA of 1.555 mg lyophilized AgNP@SDDC under the conditions mentioned above. As a control, we also performed the TGA of SDDC. In addition, we collected the Raman spectra and XPS for the AgNP@SDDC.

### *2.6 Catalytic activity of AgNP@SDDC*

To test the catalytic performance of AgNP@SDDC, we chose the reduction of *p*-nitrophenol as a model reaction. In a 1.0 cm path length cuvette, we added AgNP@SDDC (106; 211 or 314 pM) to a solution containing 59.2 μM 4-nitrophenol (4-NPh) and 181 or 195 mM $NaBH_4$. At these conditions, we supposed the reaction rate is already zero order respect to $NaBH_4$ [26]. Then, we monitored the absorption spectra over time until the band at 400 nm disappeared completely. Once we confirmed the reaction occurred, we ran kinetics at 400 nm over time at 25.0ºC and 2 seconds intervals using the kinetics mode in the instrument software. Each experiment was done in triplicate. As control experiments, we carried out the reaction in the absence of AgNP; in the absence of $NaBH_4$ and in the presence of only SDDC.

## 3. Results and Discussion

### *3.1 Synthesis and characterization of AgNP@SDDC*

We performed the synthesis of AgNP using SDDC above its critical micelle concentration in water (cmc: 0.28 mM at pH 7.00; 0.35 mM at pH 9.16) [25] to act as both a template and stabilizer, maintaining a molar ratio $Ag^+$: SDDC equal to 1:10. This ratio was chosen on basis to previous experiments performed in our laboratory to find optimal conditions for the study of the interaction of cations with Gemini surfactants. Colourless aqueous solutions of $Ag^+$ and SDDC turned to transparent brownish dispersions upon the addition of sodium borohydride. Extinction spectra of the as-synthesized AgNP showed a maximum peak attributed to the characteristic surface plasmon resonance band (SPR) for AgNP [1] at 454 nm wavelength which after centrifugation shifted to 417 nm and presented a narrower band (Fig. 1, left). TEM images of centrifuged particles (Fig. 1, right) showed nearly spherical shape with an average size of 12 nm (standard deviation, sd = 3). The zeta potential of these particles was -27 mV. We monitored the SPR over time for centrifuged AgNP@SDDC samples stored at room temperature (Fig. S1 in the Supplementary material) and observed a slight increase in absorption together with a narrower blue shifted SPR (417 to 411 nm). Despite the wavelength was shorter, their average size showed a significant increase ($p < 0.05$) to 17 nm (sd= 4) without aggregation (Fig. S2 in the Supplementary material). We attribute this increment in the mean diameter to the well-known Ostwald ripening effect [27]. In comparison to other anionic Gemini surfactants where obtained particles were in the order of microns [24], or aggregates larger than 100 nm [23], using SDDC lead to well-dispersed spherical nanoparticles of small size.

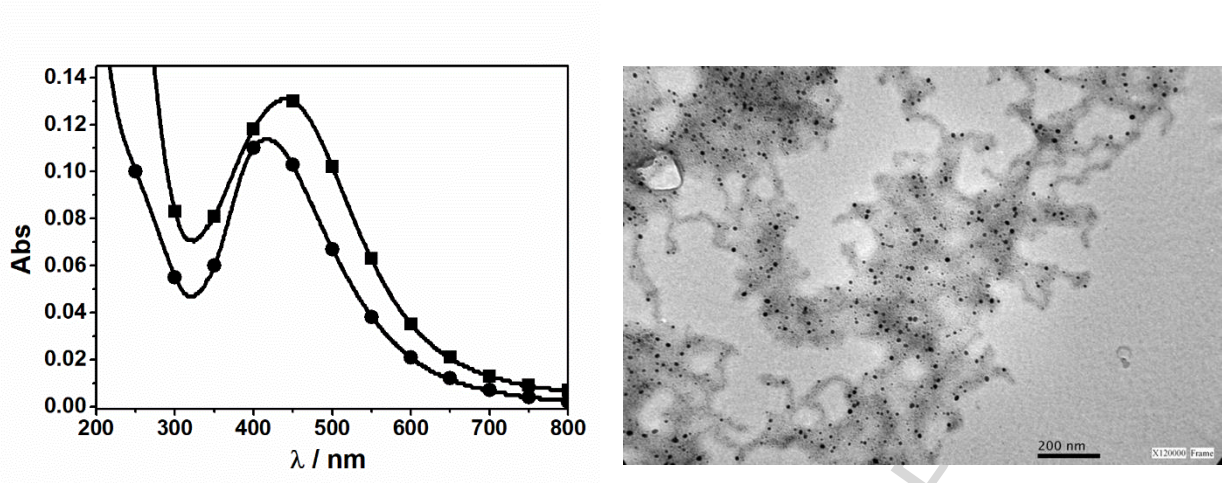


**Figure 1.** (Left) Absorption spectra for as-synthesized (■) and centrifuged (●) AgNP@SCCD colloidal suspensions in water at 25.0ºC. (Right) Representative TEM image obtained for centrifuged AgNP@SDDC. The background debris is attributed mainly to the remaining surfactant.

We determined the molar absorption coefficient (ε) in water for these AgNP@SDDC after 15 days at 411 nm obtaining a value of $(4.2 \pm 0.7)\times10^{8}$ $M^{-1}$ $cm^{-1}$ when the nanoparticle concentrations were estimated using the NANoPoLC algorithm [28] with minor modifications. Note that this algorithm takes into account the nanomaterial polydispersity. If polydispersity is not considered [29], the obtained ε is $(3.6 \pm 0.7)\times10^{8}$ $M^{-1}$ $cm^{-1}$. Addition of up to 10% v/v ethanol does not modify the ε significantly ($[4 \pm 1] \times10^{8}$ $M^{-1}$ $cm^{-1}$ at 410 nm).

To gain insight into the role as a ligand of SDDC, we collected the FT-IR spectrum of the AgNP@SDDC (Fig. 2), which displayed signals attributed to SDDC. For example, the N-H stretching vibration (secondary amide) at 3177 $cm^{-1}$, the C=O stretching at 1628 $cm^{-1}$ (amide I band), the N-H deformation mixed with the C-N stretching at 1530 $cm^{-1}$ (amide II band) and the antisymmetric and symmetric carboxylate stretching at 1584 $cm^{-1}$ and 1397 $cm^{-1}$, respectively [30]. An analysis of the ratios between peak intensities in the SDDC spectrum compared to those in the AgNP@SDDC spectrum revealed differences greater than 40%, mainly for vibrations involving the

amide and carboxylate groups (Table 1). These dissimilarities presumably are due to the interaction between SDDC with the metal surface occurring through these functional groups.

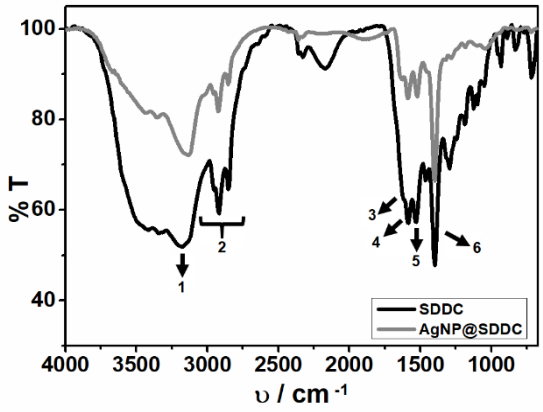


**Figure 2.** FT-IR spectra for AgNP@SDDC (grey) and SDDC (black). Arrows indicate the main vibrations bands analysed in Table 2.

**Table 1.** Selected FT-IR vibrations ($cm^{-1}$) for SDDC and AgNP@SDDC

| Entry | Band | Assignation | Rel.$^{SDDC}$ | Rel.$^{AgNP@SDDC}$ | %Δ[a] |
|---|---|---|---|---|---|
| 1 | 3177 | $\nu_{N-H}$ secondary amide | - | - | - |
| 2 | 3000-2750 | $\nu_{C-H}$ alkyl | - | - | - |
| 3 | 1628 | $\nu_{C=O}$ (Amide I) | 0.84[b] | 0.71[b] | 15 |
| | | | 0.85[c] | 0.74[c] | 13 |
| | | | 0.64[d] | 0.28[d] | 56 |
| | | | 0.71[e] | 0.35[e] | 51 |
| 4 | 1584 | $\nu_{asC=O}$ carboxylate | 1.00[c] | 1.04[c] | 4 |
| | | | 0.76[d] | 0.40[d] | 53 |
| | | | 0.85[e] | 0.50[e] | 41 |
| 5 | 1530 | $\delta_{N-H}$ mixed with $\nu_{C-N}$ (Amide II) | 0.76[d] | 0.39[d] | 51 |
| | | | 0.84[e] | 0.45[e] | 53 |
| 6 | 1397 | $\nu_{sC=O}$ carboxylate | 1.11[e] | 1.24[e] | 12 |

[a]Difference between Rel.$^{SDDC}$ and Rel.$^{AgNP@SDDC}$ expressed in percentage. [b]Relative absorption of this band with respect to band 4. [c]Relative absorption of this band with respect to band 5. [d]Relative absorption of this band with respect to band 6. [e]Relative absorption of this band with respect to band 1.

To estimate the AgNP@SDDC composition, we performed a thermogravimetric analysis. The thermogram (Fig. 3) shows a noticeable mass change (47%) between 200ºC and 400ºC

attributed to the SDDC loss and 50% of residue corresponding to the metal content. Then, we estimated a ligand density for 12 nm particles around 11800 SDDC molecules per AgNP. This high-density packing (normalized surface coverage is 27 molecules per $nm^2$, see the Supplementary material for calculus details) is likely attributable to a monodentate vertical configuration of SDDC on the nanoparticle surface (Fig. 4) instead a bidentate binding [31].

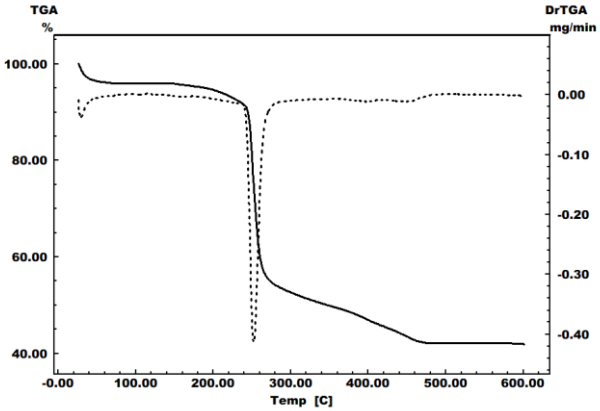


**Figure 3**. TGA (—) and corresponding DTG (---) curves for lyophilized AgNP@SDDC under $N_2$. The heating rate was 10ºC/min.

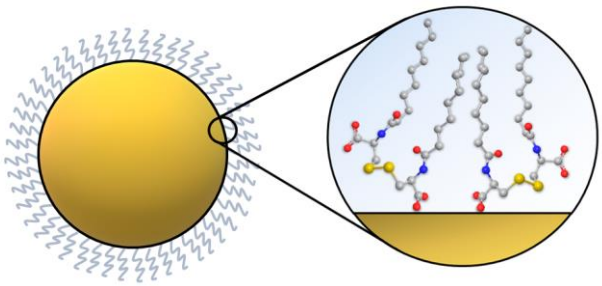

**Figure 4**. Graphical presentation of the proposed model of SDDC adsorption on the metal surface suggested on the basis of the combined information obtained from TGA and SERS data. This monodentate binding model through one carboxylate moiety was deduced from the TGA and SERS data shown in the present work and does not correspond to theoretical calculations.

We also obtained the XPS spectra to get more in-depth information on the AgNP composition. The occurrence of carbon, nitrogen, oxygen and sulphur signals (Fig. 4A-E) confirms the presence of SDDC on the AgNP surface. The C 1s spectrum (Fig. 5A) shows two peaks with binding energies 284.8 eV and 287.9 eV assigned to --$CH_2$/-C-C- and $(-COO)^-$, respectively[32]. The N 1s (Fig. 5B) and O 1s (Fig. 5C) high-resolution spectra show peaks at 400.0 eV and 531.2 eV attributable to -NH and $(O-C-O)^-$, correspondingly. In Figure 5D, the observed two peaks at 368.3 eV and 374.3 eV correspond to Ag $3d_{5/2}$ and Ag $3d_{3/2}$, respectively [18]. For its part, the high-resolution S 2p spectrum (Fig. 5E) presents two peaks at 163.2 eV and 164.4 eV consistent with the cystine disulfide chemical bond and consequently assigned to S $2p_{3/2}$ and S $2p_{1/2}$ [32].

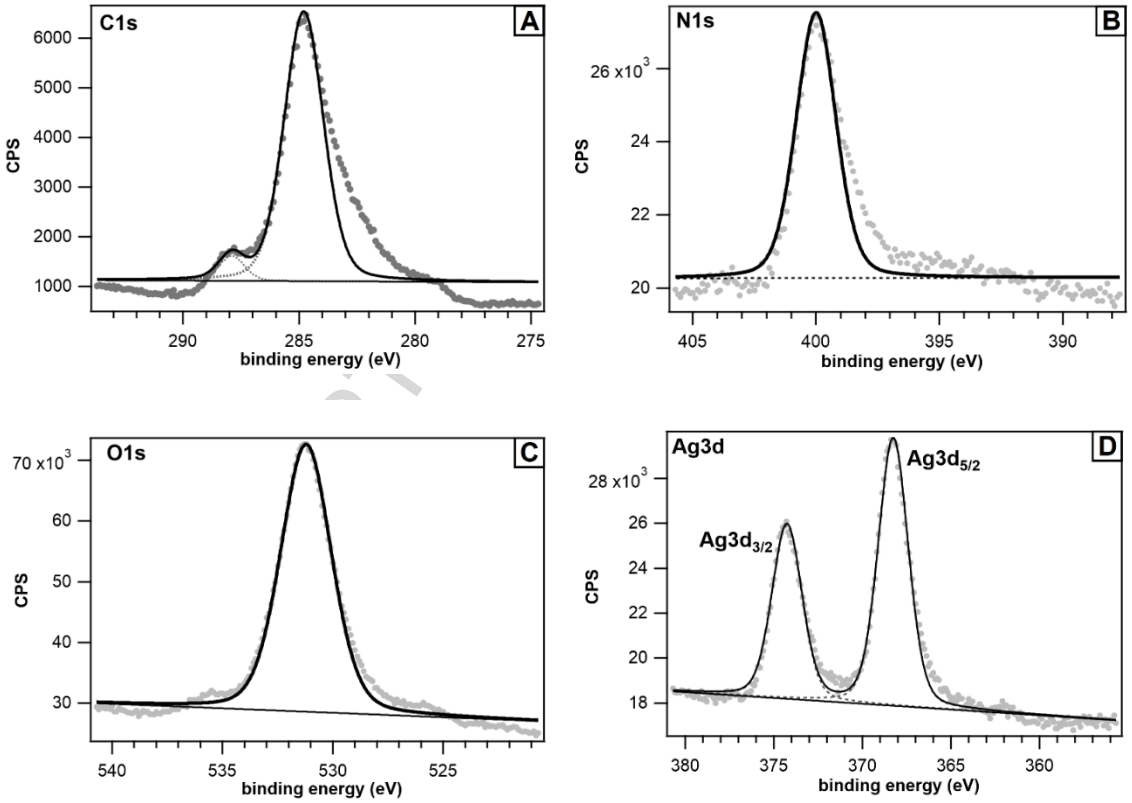


**Figure 5.** High-resolution XPS spectra of lyophilized AgNP@SDDC for C 1s (A), N 1s (B), O 1s (C), Ag 3d (D) and S 2p (E). The tail

observed at lower energies is due to charging effects, then binding energies have been corrected using the C-C (aliphatic) at 284.8 eV as a reference.

Recently, it has been demonstrated for cystine that the cleavage of the S-S bond can take place (dependent on Cys-Cys concentration) when interacting with AgNP [31]. Thus, to confirm the preservation of the S-S bond on the AgNP surface, we obtained both, the Raman and SERS spectra for SDDC and AgNP@SDDC, respectively. The appearance of a medium-strong signal around 500 $cm^{-1}$ is characteristic of the S-S stretching [33], observed at 512 $cm^{-1}$ for SDDC and around 476 $cm^{-1}$ for AgNP@SDDC (Fig. 6). Besides, the peaks in the SDDC Raman spectrum at 1371 $cm^{-1}$ and 668 $cm^{-1}$ are attributed to the carboxylate, symmetric (in phase) C=O stretching and the C-S stretching, respectively. In the AgNP@SDDC spectrum, the conservation of the S-S bond together with the observed enhancement of the C=O stretching signal, compared to the almost null C-S stretching peak, agrees with a monodentate vertical binding involving one carboxylate group and with the S-S group placed away from the metal surface (Fig. 4). The lower wavenumber observed in AgNP@SDDC for the ν(S-S) is likely a result of a strained S-S conformation. This strain is probably a consequence of the tight packing of SDDC on the nanoparticle surface [31].

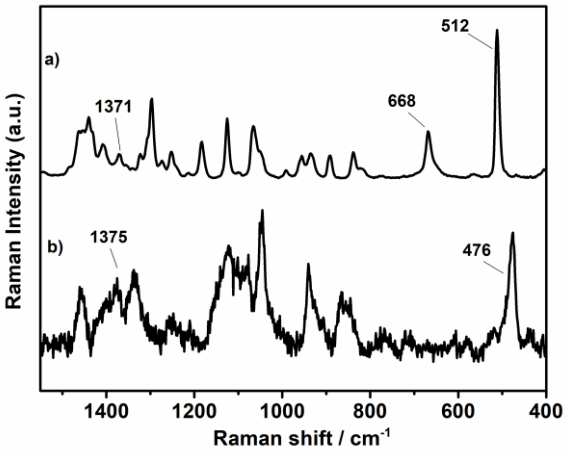


**Figure 6.** Normal Raman and SERS spectra: (a) normal Raman spectrum of SDDC powder deposited on a cover slip (excitation at 514 nm); (b) SERS spectra of lyophilized AgNP@SDDC (excitation at 633 nm).

### *3.2 Seed-mediated growth of AgNP*

As previously mentioned, surfactants usually exert control on nanoparticle morphologies [10]. For example, the seed-mediated growth of AgNP@citrate in the presence of cetyl trimethyl ammonium bromide (CTAB) produce nanorods [34]. Then, we speculated if SDDC is also able to induce any shape modification. To accomplish that, we employed as seeds 3 nm AgNP@citrate and non-centrifuged AgNP@SDDC. The reaction of these seeds for 48 hours in the growth solution lead to remarkable differences in the products depending on the type of precursor used as described below.

Using the method reported in the literature to get Ag nanorods [34], but replacing CTAB by SDDC, we observed that in the absence of $Br^-$, AgNP grew as anisotropic particles (~90 nm, sd=13; Fig. S3 in the Supplementary material). Then, the addition of bromide ions (50 mM to 100 mM) changed the proportion of different morphologies but produced nonsignificant differences on size between samples. For example, at 50 mM KBr (Fig. S4 in the Supplementary material) we observed 94% spheres (62 nm, sd=13) and 6% planar triangles (61 nm height, 57 nm length; sd=9) whereas at 100 mM KBr we observed mainly spheres (72 nm, sd=21).

By the contrary, when the seeds were AgNP@SDDC, analysis of TEM images (Fig. S5 in the Supplementary material) revealed the product was spherical silver nanoparticles of similar average size compared to the initial AgNP@SDDC (7 nm and 10 nm for 2h and 24h seeds, respectively). The absorbance change observed (Fig. 7) for the reaction product compared to the AgNP@SDDC seeds indicated the production of new AgNP@SDDC have occurred. In the presence of $Br^-$, nanorods (aspect ratio: 9.4; 9%) and bigger spheres (33 nm, sd: 9; 91%) were the growth products (Fig. S6 in the Supplementary material).

From these observations we highlight that: (I) AgNP@SDDC catalyses the reduction of $Ag^+$; (II) SDDC induces to some extent a morphology and size control and (III) $Br^-$ is likely acting as co-director in the growth process.

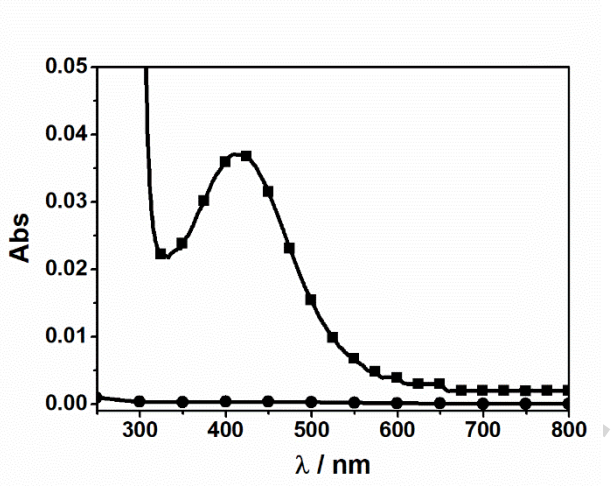


**Figure 7.** Absorption spectra for AgNP@SDDC seed dilution before (●) and after 48h reaction in the growth medium (■) at 25.0ºC.

### *3.3 Catalytic performance of AgNP@SDDC*

To get further evidence of the catalytic potential of the AgNP@SDDC, we used as a model reaction the reduction by sodium borohydride of *p*-nitrophenol (4-NPh) to the corresponding 4-aminophenol (4-APh). This reaction has been widely studied with metallic nanoparticles as it is easily followed using a UV-visible spectrophotometer [26,35–39]. The absorption band at 400 nm for the nitrophenolate anion ($4\text{-NPhO}^-$) decreases over the conversion to 4-APh which absorption is around 300 nm.

No reduction occurred in the absence of metal nanoparticles for at least six hours under our experimental conditions (Fig S7 in the supplementary material). In the presence of 11 nm AgNP@SDDC (211 pM taking into account polydispersity), the absorbance of $4\text{-NPhO}^-$ at 400 nm decreased (Fig. 8) with full conversion taking place in 30 minutes. The absence of a clear isosbestic point indicates the reaction involves more than one step to get the final product. This fact was also pointed out by Souza *et al*. with PtNP@zwitterionic surfactant [39].

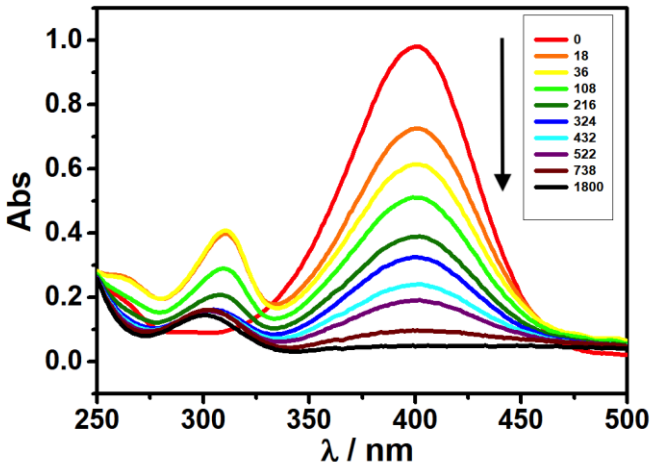


**Figure 8.** Absorption spectra over time of 4-NPh reduction by $NaBH_4$ in the presence of 211 pM AgNP@SDDC. Time in the inside legend is expressed in seconds and the arrow indicates the time evolution. For interpretation of the time references to colour, the reader is referred to the web version of this article.

A typical kinetics profile (Fig. 9) evidenced three regions: (i) an induction period determined by the induction time, $t_o$; (ii) and (iii) two kinetics regimes characterized by different slopes as an indication that the rate-limiting step changed. This observation agrees with the time evolution profile described by Gu *et al.* in an exhaustive kinetics analysis of this reaction (Scheme 2) [35]. According to that work, the rate constant for the stage (ii) is associated with a rate-limiting step dominated by the reaction from 4-$NPhO^-$ to 4-$HxPhO^-$. In the case of the regime (iii), a stationary state for 4-$HxPhO^-$ is assumed and its conversion to 4-APh becomes the slow step [35] . Besides, we also noticed the induction time was variable between different experiments. This fact can be associated with variations in $O_2$ concentration, a critical factor for this parameter as recently Menumerov *et al.* determined [40].

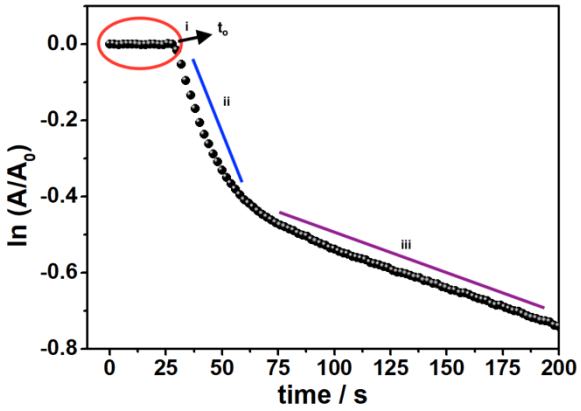


**Figure 9.** Typical time dependence observed at 400 nm wavelength for the 4-NPh reduction in the presence of 211 pM AgNP@SDDC. The red circle indicates the induction period (i) with the arrow signalling the induction time $t_o$. The blue and violet lines indicate the two different kinetics regimes (ii and iii) observed. For interpretation of the references to colour in this figure legend, the reader is referred to the web version of this article.

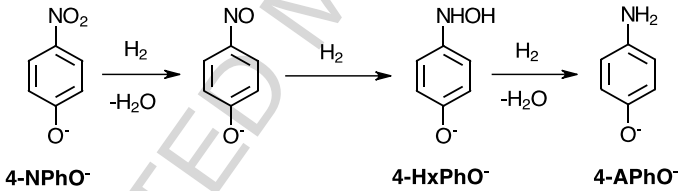


**Scheme 2.** Proposed mechanism for the 4-nitrophenol reduction by $NaBH_4$ [35].

We subtracted the delay times for each experiment and fitted the ln $(A/A_0)^{400}$ vs. time, defining the intervals corresponding to the regimes ii (0-14 s) and iii (60-168 s). Table 2 shows the calculated apparent rate constants. A rough estimation of the catalytic activity ($k_{app}$/total surface area) suggests that it is greater for step ii (~0.4 $s^{-1}m^{-2}L$) compared to step iii (~0.04 $s^{-1}m^{-2}L$) and in both cases are similar or better than for other reported AgNP [26,38]. For instance, AgNP@polymer (branched polyethyleneimine) presented a catalytic activity of 0.008 $s^{-1}$ $m^{-2}$ L or 0.57 $s^{-1}$ $m^{-2}$ L depending on the derivatized polymer [38].

After 60 min, the addition of more 4-NPh to the reaction medium showed the reduction still occurred though at a slower rate. Among other factors, as a shrinking $NaBH_4$ concentration, this might also be a result of some change on the catalyst surface. The last statement is coherent with the TEM images of the catalyst post-reaction (Fig. S8 in the Supplementary material), which show particles with an increased size and more polydisperse.

**Table 2.** Apparent rate constants determined for the different kinetics stages at 25.0ºC for different AgNP@SDDC concentrations.

| [AgNP@SDDC][a]/pM | Total surface area[b]/ $m^2$ $L^{-1}$ | *Average* $k_{app}$[c]/$10^{-3}$ $s^{-1}$ | |
|---|---|---|---|
| | | ii | iii |
| 106 | 0.0259 | 1.70 (0.03) | 1.30 (0.01) |
| 211 | 0.0515 | 12 (6) | 2.1[d] (0.5) |
| 314 | 0.0767 | 14 (3) | 1.8 (0.1) |

[a]Calculated using the NANoPoLC algorithm. [b]Estimated using the average diameter. [c]n=3, sd are in parentheses. [d]n=4.

## 4.Conclusions

In summary, silver nanoparticles have been successfully prepared using sodium didecamido cystine as the capping agent. This Gemini surfactant showed excellent properties in the synthesis, stabilization, and growth of AgNP, inducing to some extent a morphology control. We demonstrated the presence of SDDC densely packed on the nanoparticle surface, and inferred its orientation as a monodentate vertical binding, interacting mainly by the carboxylate moiety and preserving intact the disulfide bond.

The obtained AgNP@SDDC catalysed the reduction of $Ag^+$ using a mild reducing agent like ascorbic acid and SDDC acting as a nanoparticle size director to get 7-10 nm particles. This fact is remarkable different compared to other surfactants or Gemini surfactants which usually induce growth of the seeds [10,19,24]. On the other hand, the addition of KBr led to the growth of spheres and rods of the AgNP@SDDC seeds. Similar behaviour was observed with AgNP@citrate seeds, SDDC exerted some morphology control with KBr as codirector, obtaining bigger spheres and planar triangles.

Finally, AgNP@SDDC catalysed the reduction of 4-nitrophenol presenting characteristic kinetics profiles involving an induction period followed by two different kinetics regimes. Catalytic activity for the first stage is ~0.4 $s^{-1}m^{-2}L$ and for the second stage is ~0.004 $s^{-1}m^{-2}L$. These values are comparable to other reported in the literature [26,38].

Therefore, SDDC as ligand in the synthesis of silver nanoparticles generates a nanomaterial with interesting catalytic properties and it is promissory of being extended to the preparation of a variety of metal nanoparticles under appropriate conditions.

**Acknowledgements**

This work was supported in part by grants from the ANPCyT (PICT 2013-1989), the SECYT-UNC (Res. 266/16 and 113/17) and the CONICET (PIP 1122010100475CO). We thank to Dr. Claudia Nome and Dr. Valeria Quevedo (CIAP-INTA), Dr. Esteban Druetta (INFIQC-UNC) and Dr. Esteban Euti (LAMARX-FAMAF) for technical assistance with the microscopy, Raman and XPS measurements, respectively. A.M.T. and E.P.G are grateful recipient of graduated fellowships from CONICET. M.A.F, A.V.V. and N.L.P are research members of the CONICET of Argentine.

**Disclosure**

The authors declare no competing financial interests.

## 5. References

[1] E.I. Alarcón, M. Griffith, K. Udekwu, eds., Silver Nanoparticle Applications. In the Fabrication and Design of Medical and Biosensing Devices., Springer International Publishing, Switzerland, 2015.

[2] D. Pozo Perez, ed., Silver Nanoparticles, InTech, India, 2010.

[3] A. Smith, K. Johnston, S. Crawford, L. Marbella, J. Millstone, Ligand density quantification on colloidal inorganic nanoparticles, The Analyst. 142 (2017) 11–29. doi:10.1039/C6AN02206E.

[4] M.L. Nguyen, J.A. Murphy, L.C. Hamlet, B.L.T. Lau, Ligand-dependent Ag 2S formation: changes in deposition of silver nanoparticles with sulfidation, Env. Sci Nano. 46 (2018) 752. doi:10.1039/C7EN01240C.

[5] U. Tohgha, K.K. Deol, A.G. Porter, S.G. Bartko, J.K. Choi, B.M. Leonard, K. Varga, J. Kubelka, G. Muller, M. Balaz, Ligand Induced Circular Dichroism and Circularly Polarized Luminescence in CdSe Quantum Dots, ACS Nano. 7 (2013) 11094–11102. doi:10.1021/nn404832f.

[6] J.M. Abad, M. Revenga-Parra, T. García, M. Gamero, E. Lorenzo, F. Pariente, Interactions of Schiff-base ligands with gold nanoparticles: structural, optical and electrocatalytic studies, Phys. Chem. Chem. Phys. 13 (2011) 5668. doi:10.1039/c0cp02164d.

[7] H. Qi, T. Hegmann, Postsynthesis Racemization and Place Exchange Reactions. Another Step To Unravel the Origin of Chirality for Chiral Ligand-Capped Gold Nanoparticles, J. Am. Chem. Soc. 130 (2009) 14201–14206.

[8] P. Kanninen, C. Johans, J. Merta, K. Kontturi, Influence of ligand structure on the stability and oxidation of copper nanoparticles, J. Colloid Interface Sci. 318 (2008) 88–95. doi:10.1016/j.jcis.2007.09.069.

[9] M. Pisárčik, M. Lukáč, J. Jampílek, F. Bilka, A. Bilková, L. Pašková, F. Devínsky, R. Horáková, T. Opravil, Silver nanoparticles stabilised with cationic single-chain surfactants. Structure-physical properties-biological activity relationship study, J. Mol. Liq. 272 (2018) 60–72. doi:10.1016/j.molliq.2018.09.042.

[10] M.S. Bakshi, How Surfactants Control Crystal Growth of Nanomaterials, Cryst. Growth Des. 16 (2016) 1104–1133. doi:10.1021/acs.cgd.5b01465.

[11] P. Lodeiro, E.P. Achterberg, C. Rey-Castro, M. El-Shahawi, Effect of polymer coating composition on the aggregation rates of Ag nanoparticles in NaCl solutions and seawaters, Sci. Total Environ. 631–632 (2018) 1153–1162. doi:10.1016/j.scitotenv.2018.03.131.

[12] N. Mahapatra, M. Halder, Facile reversible LSPR tuning through additive-induced self-aggregation and dissemination of Ag NPs: role of cyclodextrins and surfactants, RSC Adv. 4 (2014) 18724–18730. doi:10.1039/C4RA01523A.

[13] L. Lysyakova, N. Lomadze, D. Neher, K. Maximova, A.V. Kabashin, S. Santer, Light-Tunable Plasmonic Nanoarchitectures Using Gold Nanoparticle–Azobenzene-Containing Cationic Surfactant Complexes, J. Phys. Chem. C. 119 (2015) 3762–3770. doi:10.1021/jp511232g.

[14] F.M. Menger, J.S. Keiper, Gemini Surfactants, Angew. Chem. Int. Ed. 39 (2000) 1906–1920. doi:https://doi.org/10.1002/1521-3773(20000602)39:11%3C1906::AID-ANIE1906%3E3.0.CO;2-Q.

[15] H. Fan, F. Han, Z. Liu, L. Qin, Z. Li, D. Liang, F. Ke, J. Huang, H. Fu, Active control of surface properties and aggregation behavior in amino acid-based Gemini surfactant systems, J. Colloid Interface Sci. 321 (2008) 227–234. doi:10.1016/j.jcis.2008.01.039.

[16] L. Pérez, A. Pinazo, R. Pons, M.R. Infante, Gemini surfactants from natural amino acids, Adv. Colloid Interface Sci. 205 (2014) 134–155. doi:10.1016/j.cis.2013.10.020.

[17] R. Bordes, K. Holmberg, Amino acid-based surfactants – do they deserve more attention?, Adv. Colloid Interface Sci. 222 (2015) 79–91. doi:10.1016/j.cis.2014.10.013.

[18] J. Xu, X. Han, H. Liu, Y. Hu, Synthesis and optical properties of silver nanoparticles stabilized by gemini surfactant, Colloids Surf. Physicochem. Eng. Asp. 273 (2006) 179–183. doi:10.1016/j.colsurfa.2005.08.019.

[19] M.S. Bakshi, Room Temperature Surfactant Assisted Crystal Growth of Silver Nanoparticles

to Nanoribbons, J. Nanosci. Nanotechnol. 10 (2010) 1757–1765. doi:10.1166/jnn.2010.2051.

[20] S. He, H. Chen, Z. Guo, B. Wang, C. Tang, Y. Feng, High-concentration silver colloid stabilized by a cationic gemini surfactant, Colloids Surf. Physicochem. Eng. Asp. 429 (2013) 98–105. doi:10.1016/j.colsurfa.2013.03.068.

[21] S. Bhattacharya, J. Biswas, Role of spacer lengths of gemini surfactants in the synthesis of silver nanorods in micellar media, Nanoscale. 3 (2011) 2924. doi:10.1039/c1nr10141b.

[22] N.A. Negm, S.M. Tawfik, A.A. Abd-Elaal, Synthesis, characterization and biological activity of colloidal silver nanoparticles stabilized by gemini anionic surfactants, J. Ind. Eng. Chem. 21 (2015) 1051–1057. doi:10.1016/j.jiec.2014.05.015.

[23] A. Srivastava, C. Liu, H. Fang, J. Lv, W. Qiao, Interaction and binding efficiency of cationic drug chlorpheniramine maleate – anionic amino acid gemini surfactants mixture as media for the synthesis of silver nanoparticles, Colloids Surf. Physicochem. Eng. Asp. 529 (2017) 686–695. doi:10.1016/j.colsurfa.2017.06.053.

[24] Y. Cheng, X. Liu, Q. Lei, X. Li, J. Dong, Development of novel anionic Gemini surfactants and application in fabricating hierarchical silver microparticles for surface-enhanced Raman spectroscopy, J. Colloid Interface Sci. 505 (2017) 1074–1081. doi:10.1016/j.jcis.2017.06.073.

[25] L.C. Cabana Saavedra, E.M. Pachón Gómez, R.G. Oliveira, M.A. Fernández, Aggregation behaviour and solubilization capability of mixed micellar systems formed by a gemini lipoamino acid and a non-ionic surfactant, Colloids Surf. Physicochem. Eng. Asp. 533 (2017) 41–47. doi:10.1016/j.colsurfa.2017.08.011.

[26] R. Eising, A.M. Signori, S. Fort, J.B. Domingos, Development of catalytically active silver colloid nanoparticles stabilized by dextran, Langmuir. 27 (2011) 11860–6. doi:10.1021/la2029164.

[27] G.L. Hornyak, J. Dutta, H.F. Tibbals, A.K. Rao, Introduction to Nanoscience, CRC Press, Boca Raton, 2008.

[28] C. Lazurko, M. Ahumada, F. Valenzuela-Henríquez, E.I. Alarcon, NANoPoLC algorithm for correcting nanoparticle concentration by sample polydispersity, Nanoscale. 10 (2018) 3166–3170. doi:10.1039/C7NR08672E.

[29] N.L. Pacioni, M. González-Béjar, E.I. Alarcón, K.L. Mcgilvray, J.C. Scaiano, Surface plasmons control the dynamics of excited triplet states in the presence of gold nanoparticles, J. Am. Chem. Soc. 132 (2010) 6298–9. doi:10.1021/ja101925d.

[30] K. Nakanishi, P.H. Solomon, Infrared Absorption Spectroscopy, 2nd ed., Holden-Day Inc., Oakland, 1977.

[31] E. López-Tobar, B. Hernández, M. Ghomi, S. Sanchez-Cortes, Stability of the Disulfide Bond in Cystine Adsorbed on Silver and Gold Nanoparticles As Evidenced by SERS Data, J. Phys. Chem. C. 117 (2013) 1531–1537. doi:10.1117/12.851078.

[32] R.C.M. Salles, L.H. Coutinho, A.G. da Veiga, M.M. Sant'Anna, G.G.B. de Souza, Surface damage in cystine, an amino acid dimer, induced by keV ions, J. Chem. Phys. 148 (2018) 045107. doi:10.1063/1.5011816.

[33] P. Larkin, Infrared and Raman Spectroscopy, 2nd ed., Elsevier Ltd., The Netherlands, 2018.

[34] Jana, N.R., Gearheart, L., Murphy, C.J., Wet chemical synthesis of silver nanorods and nanowires of controllable aspect ratio, Chem. Commun. (2001) 617–618. doi:10.1039/b100521i.

[35] S. Gu, S. Wunder, Y. Lu, M. Ballauff, R. Fenger, K. Rademann, B. Jaquet, A. Zaccone,

Kinetic Analysis of the Catalytic Reduction of 4-Nitrophenol by Metallic Nanoparticles, J. Phys. Chem. C. 118 (2014) 18618–18625. doi:10.1021/jp5060606.

[36] G. Hallett-Tapley, C.-O.L. Crites, M. González-Béjar, K.L. McGilvray, J.C. Netto-Ferreira, J.C. Scaiano, Dry photochemical synthesis of hydrotalcite, γ-Al2O3 and TiO2 supported gold nanoparticle catalysts, J. Photochem. Photobiol. Chem. 224 (2011) 8–15. doi:10.1016/j.jphotochem.2011.08.013.

[37] S. Wunder, F. Polzer, Y. Lu, Y. Mei, M. Ballauff, Kinetic Analysis of Catalytic Reduction of 4-Nitrophenol by Metallic Nanoparticles Immobilized in Spherical Polyelectrolyte Brushes, J. Phys. Chem. C. 114 (2010) 8814–8820. doi:10.1021/jp101125j.

[38] A.M. Signori, K. de O. Santos, R. Eising, B.L. Albuquerque, F.C. Giacomelli, J.B. Domingos, Formation of Catalytic Silver Nanoparticles Supported on Branched Polyethyleneimine Derivatives, Langmuir. 26 (2010) 17772–17779. doi:10.1021/la103408s.

[39] F.D. Souza, H. Fiedler, F. Nome, Zwitterionic Surfactant Stabilized Palladium Nanoparticles as Catalysts in Aromatic Nitro Compound Reductions, J Braz Chem Soc. 27 (2016) 372–381.

[40] E. Menumerov, R.A. Hughes, S. Neretina, Catalytic Reduction of 4-Nitrophenol: A Quantitative Assessment of the Role of Dissolved Oxygen in Determining the Induction Time, Nano Lett. 16 (2016) 7791–7797. doi:10.1021/acs.nanolett.6b03991.

**Graphical Abstract**

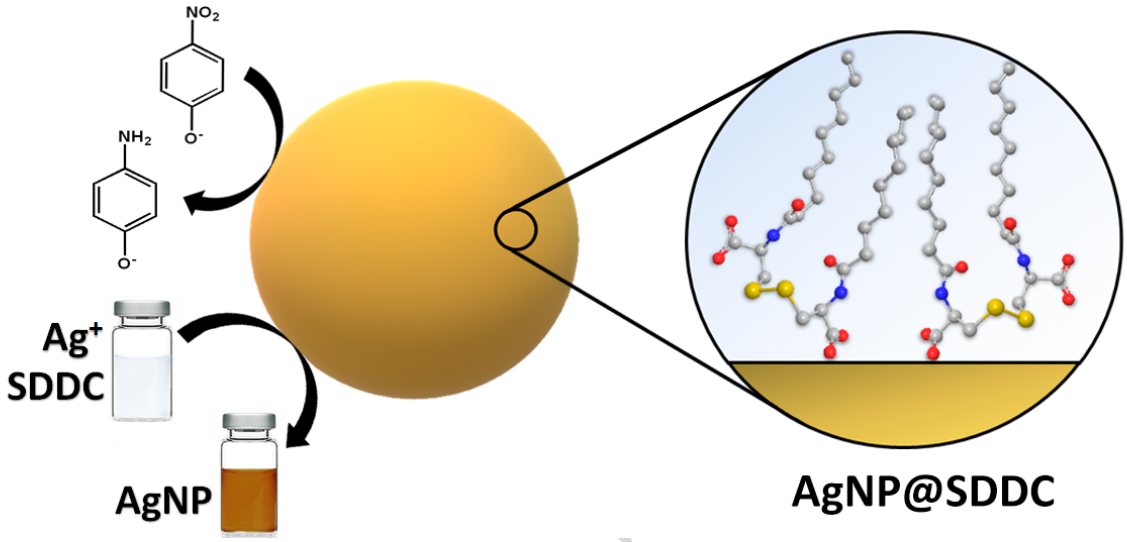

HIGHLIGHTS

- A Gemini lipoamino acid surfactant as ligand lead to stable silver nanoparticles
- A monodentate vertical binding through the carboxylate group to the metal surface
- Synthesized AgNP@SDDC are catalytically active to the p-nitrophenol reduction
- The size of AgNP@SDDC seeds is kept constant during the seed-mediated growth